Slab-selective, BOLD-corrected VASO at 7 tesla provides measures of cerebral blood volume reactivity with high signal-to-noise ratio.

Magnetic Resonance in Medicine 72:137–148 (2014)

Slab-Selective, BOLD-Corrected VASO at 7 Tesla Provides Measures of Cerebral Blood Volume Reactivity with High Signal-to-Noise Ratio

Laurentius Huber,[1]* Dimo Ivanov,[1,2] Steffen N. Krieger,[1,3] Markus N. Streicher,[1] Toralf Mildner,[1] Benedikt A. Poser,[2,4,5] Harald E. Möller,[1] and Robert Turner[1]

Purpose: MRI methods sensitive to functional changes in cerebral blood volume (CBV) may map neural activity with better spatial specificity than standard functional MRI (fMRI) methods based on blood oxygen level dependent (BOLD) effect. The purpose of this study was to develop and investigate a vascular space occupancy (VASO) method with high sensitivity to CBV changes for use in human brain at 7 Tesla (T).

Methods: To apply 7T VASO, several high-field-specific obstacles must be overcome, e.g., low contrast-to-noise ratio (CNR) due to convergence of blood and tissue T_1, increased functional BOLD signal change contamination, and radiofrequency field inhomogeneities. In the present method, CNR was increased by keeping stationary tissue magnetization in a steady-state different from flowing blood, using slice-selective saturation pulses. Interleaved acquisition of BOLD and VASO signals allowed correction for BOLD contamination.

Results: During visual stimulation, a relative CBV change of $28\% \pm 5\%$ was measured, confined to gray matter in the occipital lobe with high sensitivity.

Conclusion: By carefully considering all the challenges of high-field VASO and filling behavior of the relevant vasculature, the proposed method can detect and quantify CBV changes with high CNR in human brain at 7T. **Magn Reson Med 72:137–148, 2014. © 2013 Wiley Periodicals, Inc.**

Key words: vascular space occupancy; slab-selective VASO; cerebral blood volume; 7 Tesla; fMRI acquisition techniques

INTRODUCTION

A local change in cerebral blood volume (CBV) provides a quantitative physiological variable to detect neuronal activation and may localize changes of neural activity better than other variables accessible by functional MRI (fMRI), such as cerebral blood flow (CBF) and blood oxygenation level. In particular, CBV-weighted fMRI has shown higher local specificity for the distribution of neural activity across cortical layers (1,2) and location on the cortical surface (3) than the commonly used blood oxygen level dependent (BOLD) fMRI. However, the widespread use of CBV-weighted fMRI in humans is hampered due to the invasiveness of exogenous contrast-based CBV measurements and the low signal-to-noise ratio (SNR) of noninvasive CBV-weighted methods.

Vascular space occupancy (VASO) is an fMRI method that measures CBV changes noninvasively through selective detection of signal changes in the extravascular compartment concurrent with changes in the nulled blood compartment (4). The VASO contrast is based on the difference between longitudinal relaxation times (T_1) of tissue and blood. It is generated by applying an inversion pulse before signal acquisition, so as to effectively null the contribution of blood water magnetization at the time of signal excitation (so-called "blood-nulling time"), while keeping substantial tissue signal for detection. Relative changes of residual tissue signal are then associated with changes in CBV. At high magnetic field strengths, four confounding effects have hampered the implementation of VASO (5,6). First, the tissue signal at the blood-nulling time is significantly reduced due to convergence of tissue and blood T_1 values at high fields (7). This results in a contrast-to-noise ratio (CNR) for VASO that is disappointingly small. Second, the positive BOLD signal change during neural activation increasingly counteracts the negative VASO signal change (8) with increasing magnetic field strength. Third, inhomogeneities in the radiofrequency (RF) fields and safety limits concerning specific absorption rate of emitted energy hamper efficient spin inversion, which is vital for blood-nulling in VASO. The fourth issue of using VASO at high fields is the higher susceptibility to blood inflow effects, resulting from the conjunction of two characteristics of high field MRI. On one hand, the inversion volume is reduced when a head coil is used for RF transmission (which is common at 7T). This increases the likelihood of inflow of fresh blood during the blood-nulling time. On the other hand, blood-nulling time is increased at high-fields due to longer blood T_1, which further increases the possibility of inflow effects.

Confounding BOLD signal contributions can be avoided by using a very short echo time (TE) (4,9) or estimating the signal at $TE = 0$, while acquiring images at multiple TEs (8). Here, a new BOLD-correction

[1]Max Planck Institute for Human Cognitive and Brain Sciences, Leipzig, Germany.

[2]Maastricht Brain Imaging Centre, Maastricht University, Maastricht, The Netherlands.

[3]Monash Biomedical Imaging, Monash University, Melbourne, Victoria, Australia.

[4]Department of Medicine, John A. Burns School of Medicine, University of Hawaii, Honolulu, Hawaii, USA.

[5]Donders Institute, Centre for Cognitive Neuroimaging, Radboud University Nijmegen, Nijmegen, The Netherlands.

*Correspondence to: Laurentius Huber, M.Sc., Nuclear Magnetic Resonance Unit, Max Planck Institute for Human Cognitive and Brain Sciences, Stephanstrasse 1 A, 04103 Leipzig, Germany. E-mail: lhuber@cbs.mpg.de

Received 6 March 2013; revised 4 July 2013; accepted 16 July 2013

DOI 10.1002/mrm.24916

Published online 20 August 2013 in Wiley Online Library (wileyonlinelibrary.com).

mechanism is presented. To assess and eliminate BOLD contributions, data without blood nulling (i.e., with signal changes entirely based on the BOLD effect) are acquired, interleaved with BOLD-contaminated VASO data. The almost simultaneously detected BOLD signal thus permits straightforward correction of the VASO signal.

Potential methods to increase tissue *z*-magnetization at the time when blood water magnetization is nulled have been proposed in several studies. Tissue signal can be increased by up to a factor of 1.5 using an off-resonant magnetization transfer pulse (6,10). The signal can also be increased by manipulating the steady-state *z*-magnetization with adaptations in the repetition time (TR) and inversion time (TI) of the inversion recovery sequence (5,11–13).

Jin and Kim showed that blood *z*-magnetization cannot approach steady-state during TR at high fields, where the blood nulling time is long and no body-coil is typically available (14). They suggested that the blood magnetization should be considered not to be in steady-state, and to adjust the blood-nulling time accordingly. The blood *z*-magnetization can be maintained in this non–steady-state by inverting the blood only in a slab within the volume included by the coil coverage. Simulations of this slab-inversion VASO (SI-VASO) showed that the resulting signal tissue can be significantly increased (5). Corresponding measurements in anesthetized cats at 9.4T showed improved cortical-layer specificity compared with spin-echo BOLD (5). To avoid inflow of fresh blood in cat SI-VASO, however, blood signal is not nulled, so that the SI-VASO sequence becomes like a FAIR sequence (15) without a control condition and with an TI few hundred ms before blood nulling. Quantitative estimation of CBV changes and distinguishing between blood flow and volume changes become difficult.

Following the method of Jin and Kim (5), we implemented a slab-selective inversion pulse and applied SI-VASO in humans with potentially higher SNR compared with original VASO. In human brain at 7T, the time for blood to flow from the lower bound of the inversion slab into the microvessels of the imaging slice ("arterial arrival time") is similar to the blood-nulling time. This enables TI, the inversion efficiency, and the inversion slab thickness to be mutually adjusted, so that all blood in the microvasculature is nulled, thus reducing potential inflow contamination of the VASO contrast. To further increase gray matter (GM) magnetization at the blood-nulling time, the steady-state of stationary tissue magnetization was arranged to be maximal at the nulling time of nonsteady-state flowing blood. This could be achieved by applying additional 90° RF pulses in the imaging slice shortly before slab-selective inversion. The low tissue *z*-magnetization at the time of inversion results in a large *z*-magnetization at the subsequent blood-nulling time TI. These 90° RF saturation pulses are also used to flip the tissue magnetization into the transverse plane within the BOLD signal acquisition module. We describe this technique as slice-saturation slab-inversion VASO or SS-SI-VASO.

The anticipated increase in functional CNR SS-SI-VASO, despite the aforementioned obstacles of high-field VASO, may be used to improve the spatial resolution of CBV change measurements in healthy human brains.

THEORY

Sequence Design

The pulse sequence diagram and the associated relative *z*-magnetization of once-inverted blood, GM, and cerebrospinal fluid (CSF) are depicted in Figure 1. Tissue signal increase in SS-SI-VASO is achieved by manipulating the *z*-magnetization of flowing blood differently from that of stationary GM. As detailed below, inversion slab thickness, inversion efficiency, inversion times TI1 and TI2, and TR are adjusted such that two conditions are fulfilled. These are (a) no noninverted blood should enter the microvasculature of the imaging region during TI1, and (b) microvasculature of the imaging slice should be completely refreshed by spins outside the violet slice of Figure 1c between TI2 of the previous TR and TI1 of the of the present TR. The higher tissue signal in SS-SI-VASO comes primarily from the fact that, due to the previous excitation pulse, the stationary GM *z*-magnetization is very small at the time of inversion, thus it is higher at the subsequent image acquisition. An additional signal increase comes from the fact that the blood nulling time of once-inverted blood magnetization is longer compared with steady-state blood, providing the *z*-magnetization of the neighboring tissue more time to undergo longitudinal relaxation.

Inflow of Noninverted Blood Magnetization

The nulling time of once-inverted blood magnetization is given by $TI1 = (\ln 2)\, T_{1,\mathrm{blood}}$, which yields approximately 1450 ms at 7 Tesla (T) ($T_{1,\mathrm{blood}}$ is the T_1 of blood water), assuming $T_{1,\mathrm{blood}} = 2100$ ms (16–19). The inversion slab must be thick enough that no noninverted ("fresh") blood magnetization reaches the imaging slice during that time. In humans, it takes approximately 1000–1400 ms until blood from the upper neck region reaches the larger vessels of the occipital lobe (20,21). Furthermore, it takes another 400–500 ms until fresh blood reaches the small arterioles that dynamically change their diameter during activation (21). These numbers suggest that the blood-nulling time is shorter than the arterial arrival time of fresh blood, and it takes longer than TI1 for noninverted blood magnetization to arrive in the microvasculature of the imaging slice.

The SS-SI-VASO technique can also be applied in brain regions with significantly shorter arterial arrival times, by reducing the blood-nulling time TI1. A convenient way to make the blood-nulling TI1 shorter is to reduce the inversion efficiency of the (adiabatic) preparation pulse. To achieve this, the concept of RF phase modulation during the RF pulse was applied. Such phase modulations are known from plane rotation pulses for flip-angle variations (22) and are transferred to conventional adiabatic pulses here. The reduction in inversion efficiency is achieved here by introducing a phase

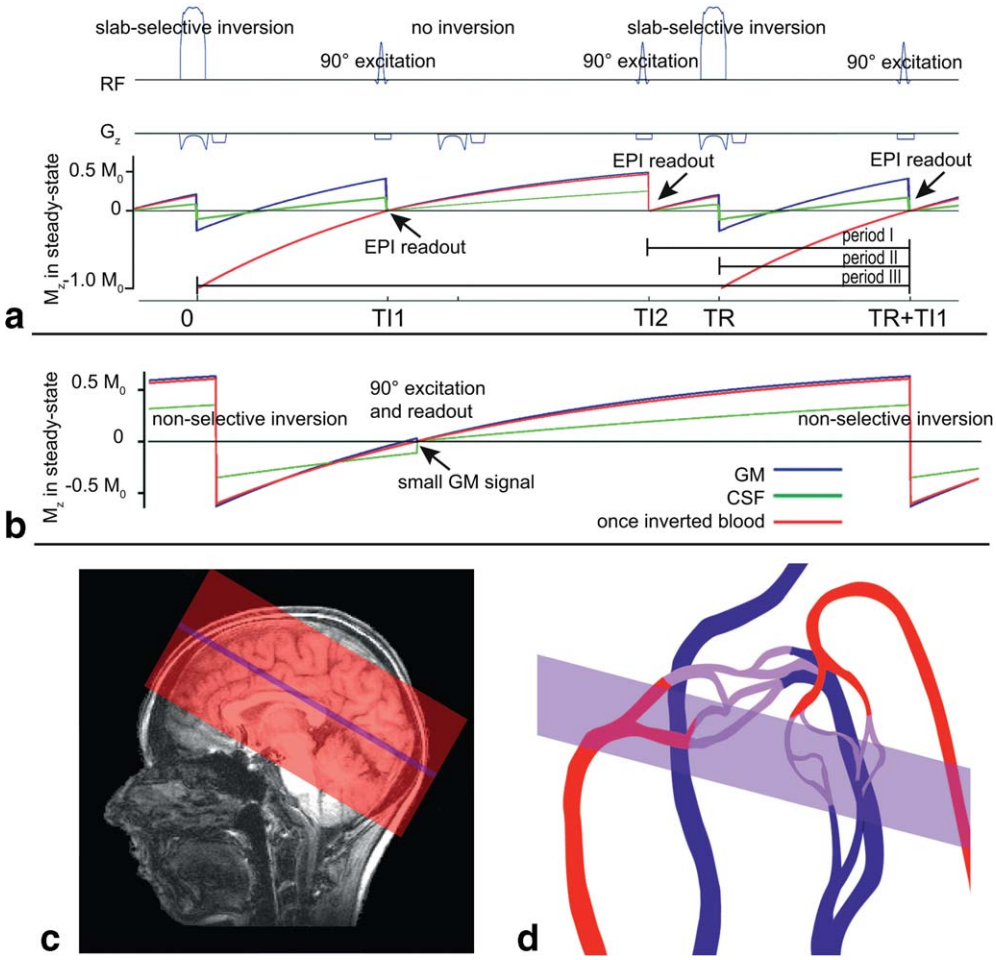

FIG. 1. **a**: Sequence diagram and the corresponding steady-state *z*-magnetization of GM, CSF, and blood in SS-SI-VASO. The depicted blood component refers to once-inverted blood *z*-magnetization. Therefore, blood *z*-magnetization is $-M_0$ after inversion, independent of the magnetization before inversion. **b:** Depicts the expected *z*-magnetization of blood and GM in original VASO. Due to similar T_1, GM *z*-magnetization is very small at the blood-nulling time. **c:** Depicts schematically the geometry of inversion slab and imaging slice. The nulling condition requires that the (violet) imaging slice is refilled with nonsaturated blood during period I. Furthermore, it is required that no blood outside of the (red) inversion slab flows into the microvasculature of the (violet) imaging slice during period II. Additionally to the refilling condition of the imaging slice during period I, the inversion slab (red) should be refilled with fresh blood during period III. **d:** Illustrates how the vasculature of the imaging slice is refilled during consecutive 90° pulses. Even though, it contains arterial, capillary, and venous compartments, the refilling time can be much shorter that the refilling time of the total vascular tree.

skip of the RF field B_1 during the inversion at the time when the frequency of the adiabatic pulse is exactly on resonance. This opens the "cone of precession" of the magnetization that precesses around the effective magnetic field during inversion. After inversion, the cone of precession points along the negative *z*-direction. The B_1-independent reduction in inversion efficiency is then given by the transverse component of the magnetization, which depends directly on the phase skip applied.

Outflow of Blood that Has Not Been Inverted Once

SS-SI-VASO captures blood that has been inverted only once, and has not experienced the previous excitation pulse. Therefore, two refilling conditions must be fulfilled. First, the period between blood-not-nulled and blood-nulled image acquisitions must be longer than the refilling time of the vasculature of the imaging slice (period I in Figure 1). Otherwise, blood magnetization that had experienced the previous excitation pulse would not be completely nulled. The macrovessels with high blood flow velocities penetrating the imaging slice are believed to be more quickly refilled than the microvasculature. Therefore, the refilling time of the microvasculature is considered in more detail. Blood velocity measurements suggest that the microvasculature is refilled in 1–1.5 s (23–25). Results of Nakagawa et al. suggest that both plasma and red cell transit times through the microvasculature are shorter than 0.5 s (26). Reviewing seven studies, the microvascular transit time was estimated to be 1.16 s (27). Therefore, it takes less than 1–2 s until the microvasculature is refilled with fresh blood that has not experienced the previous excitation pulse. The second refilling condition refers to the inversion slab (red area in Figure 1c) during period III and is discussed in Jin and Kim (5). It states that there should be no twice-

inverted blood magnetization in the imaging slice during VASO image acquisition. Note that period III is longer than TR. It can be explained with the different timing between generation of the VASO contrast by means of inversion and VASO image acquisition. Even if not all inverted blood magnetization has left the imaging slice during the next inversion pulse, it will not contribute to the MR signal as long as no image is acquired. Only if the blood magnetization still has not left the imaging slice when the following image is acquired (after period III), it is captured and contaminates the contrast.

BOLD Correction

Additional to the acquisition of BOLD-contaminated VASO signal change, BOLD signal change without VASO contamination is acquired by implementing the inversion pulse only prior every second echo-planar imaging (EPI) readout (see Figure 1a). When the BOLD contrast contribution is known, the BOLD contamination in the VASO image can be factored out.

We consider a simple model of the effect of the proposed BOLD correction. The gradient-echo signal of a voxel can be considered as the *z*-magnetization M_z in the voxel at the time of excitation multiplied with an exponential dephasing term: $S \sim M_z\ exp(-TE/T_2^*)$, where M_z depends on the relative proton density, the inversion time TI1, and the relative volume distribution of the compartments in the voxel. T_2^* denotes the transverse relaxation time in gradient echo acquisitions. If a voxel contains only blood and GM (no white matter and CSF), the signal arising only from GM during the nulling condition (nc) can be expressed as:

$$S_{GM,nc} \sim M_{z,GM,nc}\, e^{-\frac{TE}{T^*_{2,GM}}}. \quad [1]$$

VASO is based on the idea that $M_{z,GM,nc}$ changes during activity and that this change is proportional to 1-CBV. For more details about this proportionality see Lu et al (4) Eq. [4] or Lu et al (28) Eq. [2]. To obtain $M_{z,GM,nc}$, the dephasing term must be factored out, because T_2^* also changes with activation. To do so, the signal at the nulling condition is normalized to the signal that is acquired while blood is not nulled (nn). This signal can be expressed analogously as:

$$S_{par,nn} \sim M_{z,par,nn} e^{-\frac{TE}{T^*_{2,par}}} \quad [2]$$

where the *z*-magnetization of the parenchyma $M_{z,par,nn}$ contains both spins within GM and spins in blood. At the time the blood-not-nulled image is acquired, the relative *z*-magnetizations of blood and GM, and the proton densities of blood and tissue are very similar. Hence, the $M_{z,par,nn}$ term can be considered to be independent of brain activation. In other words, blood volume sensitivity is obtained only when a VASO inversion preparation is applied, and signal change in the BOLD image comes only from changes in T_2^* and not from redistribution of water magnetization between intravascular and extravascular space. Thus, we can assume that $M_{z,par,nn} \approx const$. Hence, after normalizing S_{nc} with S_{nn}, we obtain:

$$\frac{S_{nc}}{s_{nn}} = \frac{M_{z,GM,nc}\, e^{-\frac{TE}{T^*_{2,GM}}}}{const\, e^{-\frac{TE}{T^*_{2,par}}}} \approx \frac{M_{z,GM,nc}}{const} \sim 1 - CBV. \quad [3]$$

Here, it is assumed that at high field strengths the T_2^* of the parenchyma, which includes blood and tissue, is equal to the T_2^* of extravascular tissue. With this assumption, the T_2^*-weighting cancels out upon division of the signals from both acquisitions, and the resulting signal is independent of BOLD-related changes. Hence, it is assumed that the transverse relaxation is independent of the inversion time. It must also be stressed that the BOLD correction scheme can only correct for extravascular BOLD signal change, which at 7T accounts for approximately 90% of the total BOLD signal change at TE used in this study (29,30). To validate this approach experimentally, it is compared with an alternative BOLD correction method based on a multi-echo acquisition (8). Equation [3] claims only proportionality between the BOLD corrected VASO signal and CBV. According to discussions in (28), this proportionality factor depends strongly on partial voluming of CSF or WM and their T_1 contrast. Because this proportionality factor is not measured, the proposed method can be used only to estimate relative CBV changes, not to estimate absolute CBV.

METHODS

Image Acquisition

The slab-selective, BOLD-corrected pulse sequence was implemented in the IDEA programming environment on a Siemens MAGNETOM 7T scanner (Siemens Medical Solutions, Erlangen, Germany). For RF transmission and reception, a 24-channel receive and circularly polarized single-channel transmit head coil (Nova Medical, Wilmington, MA) was used. Data were acquired in five axial slices aligned along the sulcus calcarinus (thickness 1.5 mm, no slice gaps) with a two-dimensional single-shot gradient-echo EPI readout. The imaging parameters were: TE/TR = 19/3000 ms, nominal voxel size of 1.5 × 1.5 × 1.5 mm^3, partial Fourier factor 5/8. A TR-FOCI inversion pulse (31) was implemented to achieve efficient slab-selective inversion despite B_1-inhomogeneities and specific absorption rate constraints at high field. The inversion pulse duration could be reduced from the typical 15–20 ms to 5 ms, which minimized the BOLD-dependent $T_{1\rho}$ relaxation of venous blood, which might reduce inversion efficiency. The slab-selective gradient strength was adjusted to achieve an inversion slab thickness of 14.28 cm. Pilot measurements ensured that no fresh blood flows into the imaging slice during TI1 (period II in Figure 1). Because the inversion pulse is only applied before every second image, the inversion-pulse repetition time was 3 s.

Considering an inversion efficiency of 95%, as measured in pilot scans, leads to TI1 = 1330 ms for the blood-nulling time. The timing of the sequence was adjusted such that the BOLD image acquisition was always right between two consecutive VASO images. Therefore, TI2 = TI1 + TR/2 (see Figure 1a).

Further inversion recovery measurements with multiple TI1s of 36/200/300/900/1100 ms were performed

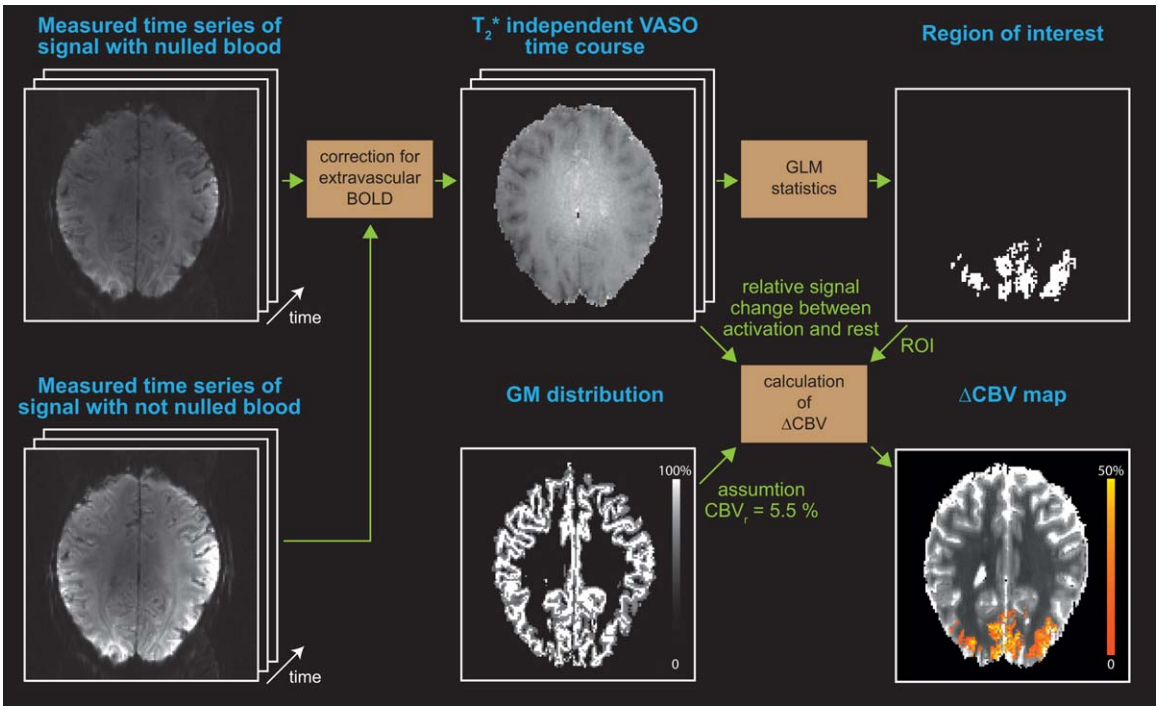

FIG. 2. Evaluation procedure for calculating ΔCBV from the measured MR time series. To factor out the T_2^* dependence of activation, motion-corrected time series of blood nulled images are normalized to motion corrected time series of images with not-nulled blood. General linear model statistics is applied to these T_2^* corrected time series to define ROIs. Signal change within these ROIs is normalized with blood volume fraction at rest, which is estimated from relative GM volume within each voxel, to calculate relative CBV change. [Color figure can be viewed in the online issue, which is available at wileyonlinelibrary.com.]

with acquisition parameters otherwise identical to the functional scans. Following the methods of Shin et al (32), these data were used to generate T_1 estimates and GM maps with distortions identical to the functional data.

Ten healthy human volunteers (five female, 23 to 33 years old) were scanned with the scan parameters described. A 6-min duration high-contrast moving starfield paradigm (block design: 30 s rest followed by 30 s stimulation) (33) was used to induce neural activation throughout the visual cortex.

To evaluate inflow effects arising from noninverted blood magnetization, three additional subjects (one female, 27 to 32 years old) were scanned during a 12-min duration hypercapnia task consisting of 2/5/5 min of breathing air/5% CO_2, 21% O_2 and balance N_2/air. The tremendous decrease of arterial arrival time during hypercapnia in the range of 10–20% (34) was used here to show how effects of inflow of fresh (noninverted) blood magnetization can be avoided by means of manipulations of the blood-nulling time. To deal with the reduced arterial arrival time during hypercapnia, the blood-nulling time was varied (TI1=1330/1120/765 ms) by adjusting the adiabatic inversion pulse efficiency to 100%, 86% and 75% in a B_1-independent way, as described above. All other sequence parameters remained unchanged.

To validate the BOLD correction method, seven additional volunteers (4 female, 22 to 30 years old) were scanned with a multi-echo EPI readout. Acquisition parameters were TE = 12/32/52 ms, partial Fourier factor = 5/8, and a nominal voxel size of 1.5 × 1.5 × 1.5 mm^3. All other sequence parameters remained unchanged.

To investigate the potential advantage of SS-SI-VASO at 3T, the sequence was also implemented on a MedSpec 30/100 whole-body scanner (Bruker Biospin, Ettlingen,

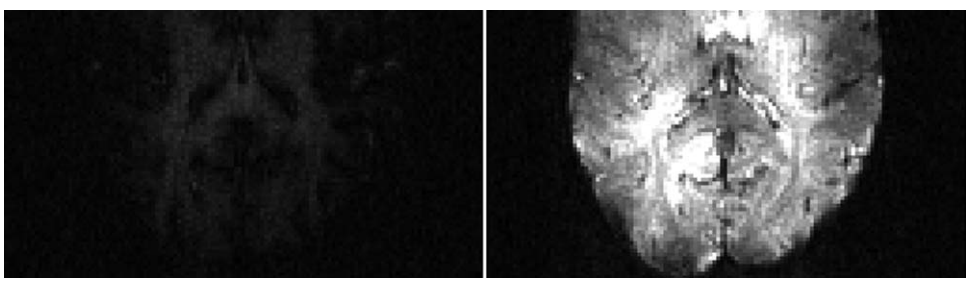

FIG. 3. Single-shot EPI images obtained at 7T with nominal voxel size of 1.5 × 1.5 × 1.5 mm^3, TR = 3 s, TI1 is 560 ms and 1330 ms for original and SS-SI-VASO, respectively. Images are scaled identically. Gray values represent signal intensities in arbitrary units.

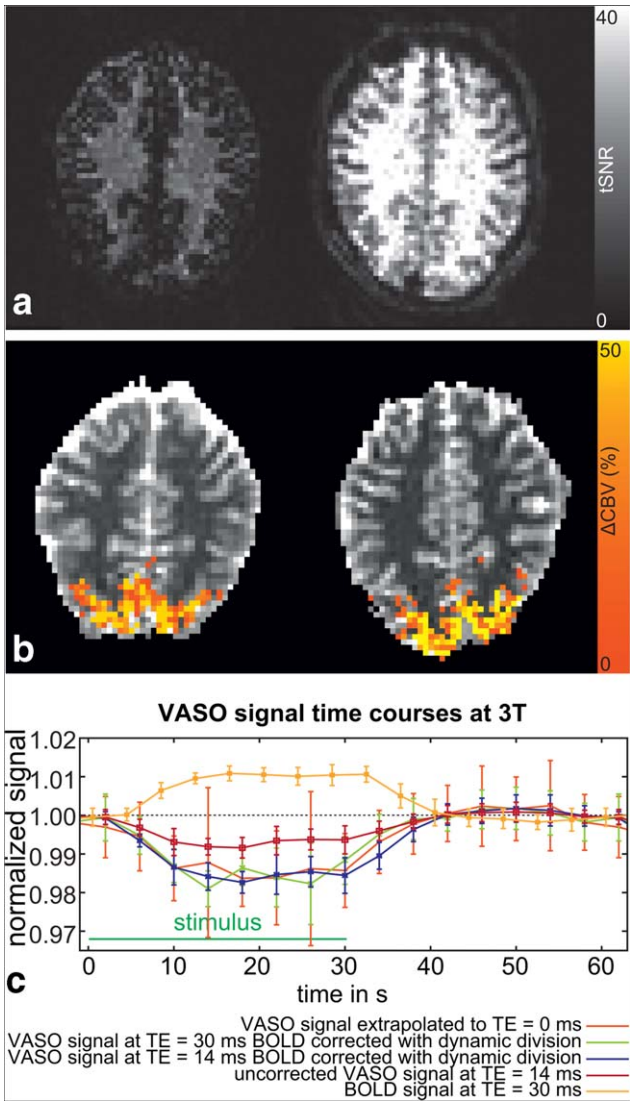

FIG. 4. Results from the two subjects at 3T. **a:** Depicts tSNR maps of original VASO with TR/TI1 = 4000/625 ms and SS-SI-VASO with TR/TI1 = 4000/1015 ms of one subject. tSNR in GM regions is 9 and 32 for original VASO and SS-SI-VASO, respectively. **b:** Depicts maps of relative CBV change in both subjects within ROIs of significant signal change. **c:** Depicts VASO signal time courses of the two subjects for different BOLD correction schemes. Error bars refer to the standard deviation between consecutive activation-rest periods. [Color figure can be viewed in the online issue, which is available at wileyonlinelibrary.com.]

Germany). A commercial birdcage head coil (Bruker Biospin) was used for RF transmission and reception. Two subjects were scanned with SS-SI-VASO parameters of TR/TI1 = 4000/1015 ms, TE = 14/30 ms, nominal voxel size = 3 × 3 × 4 mm^3. The TR-FOCI inversion pulse duration was increased to 10 ms.

All procedures of this study had been approved by the Ethics Committee of the University of Leipzig. Informed written consent was given by all volunteers.

Data Analysis

The image-evaluation procedure is illustrated in Figure 2. MR images were corrected for motion with SPM8 (Wellcome Department, University College London, London, UK). Statistical analysis was done using FSL Feat (Version 5.98) (35). Activation areas were defined with the VASO data as a cluster of voxels having Z-values above 2.3 and a significance level of $P < 0.05$ (corrected for multiple comparisons). BOLD-correction, T_1-fits and the extrapolation of signal change were processed with in-house algorithms written in C++ using ODIN-libraries (36). To scale the relative VASO signal change to relative change in CBV, blood volume at rest was estimated. Therefore, the individual GM volume of every voxel was estimated based on the T_1-fit. As in previous VASO studies, blood volume at rest (CBVr) within this GM fraction was assumed to be 5.5% (37,38). CBVr was assumed to be evenly distributed within GM. The T_1-maps were also used to generate maps of CSF. Because the nominal resolution of 1.5 mm is on the order of the cortical thickness, voxels that contain the surface layers of the cortex could be identified by the partial volume fraction of CSF.

RESULTS

Slab-selective VASO provides a larger GM signal than original VASO at 7T (Fig. 3) and at 3T (Fig. 4a). This increase results from the longer blood-nulling time (TI1) for once-inverted blood water z-magnetization, compared with steady-state blood water z-magnetization. From calculations based on the Bloch equations, the z-magnetization is expected to increase in GM by a factor of 8.7 at 7T (assuming $TR/T_{1,blood}/T_{1,GM} = 3/2.1/1.9$ s at 7T) and 3.6 for 3T (assuming $TR/T_{1,blood}/T_{1,GM} = 4/1.6/1.2$ s at 3T). This agrees well with signal increases by factors of approximately 4 and 8 observed experimentally within GM-regions at 3T and 7T, respectively.

Three slices of ΔCBV maps obtained during visual stimulation of all 10 subjects are shown in Figure 5. Widespread ΔCBV increases can be seen in GM in the visual cortex corresponding to the central visual field. The measured relative CBV changes upon visual stimulation of the depicted regions are summarized in Table 1. Figure 4b depicts results from two subjects at 3T. Similar to the 7T results, CBV increases confined to GM in the visual cortex can be seen.

Signal time courses of BOLD and VASO of the ROIs depicted in Figure 5 are shown in Figure 6. Both time courses are very similar in their dynamics. The return to baseline after stimulus cessation is on a similar time scale in BOLD and in VASO. The intersubject stability is slightly greater in VASO compared with BOLD signal, as indicated by the smaller error bars. This finding holds true independent of whether the ROIs were defined from the BOLD or VASO time courses.

The echo time dependence of BOLD and VASO signal from the multi-echo experiments is depicted in Figure 7. VASO signal time courses are shown for the two different BOLD correction methods: BOLD correction with dynamic division for two echo times and the BOLD correction from exponential extrapolation to TE = 0 ms. The latter correction method results in a larger intertrial variation associated with larger error bars, presumably due to the low SNR of the images during the later echoes. There is no significant difference in amplitude and

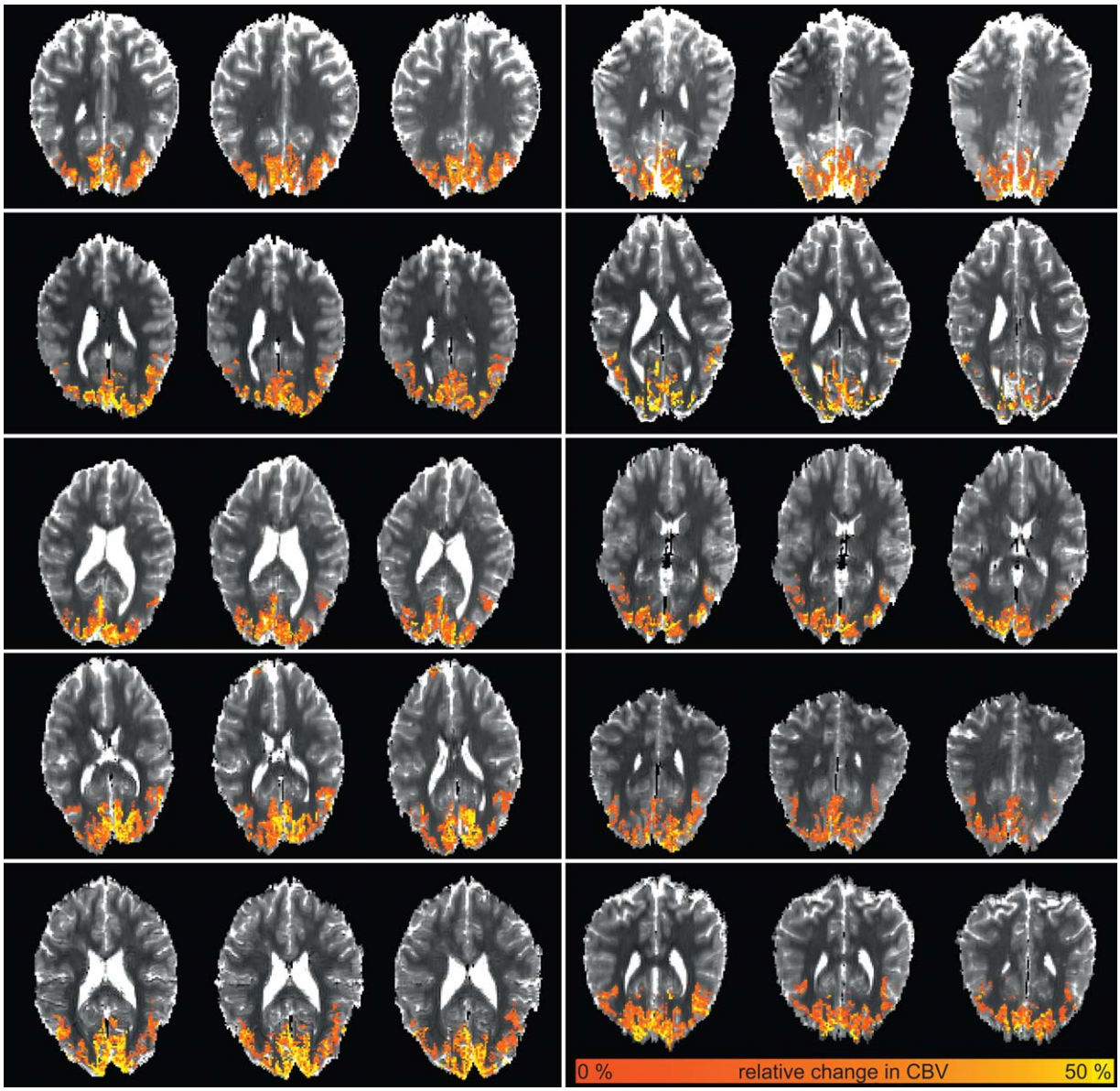

FIG. 5. Three slices of every subject scanned at 7T are shown. The change in CBV is located in the visual cortex as expected. The mean change in CBV is 28% ± 5%.

temporal dynamics between the two BOLD correction methods. The amplitude of the BOLD signal change on the other hand is highly dependent on TE, as expected.

BOLD-corrected VASO signal time courses acquired at 3T (Fig. 4c) are indistinguishable from 7T results with regard both to amplitude and temporal characteristics. VASO time courses without BOLD correction significantly underestimate CBV changes even at 3T. VASO signal time courses are independent of whether the BOLD correction was performed with dynamic division (for TE = 14 and 30 ms) or whether BOLD correction was based on exponential T_2*-extrapolation. Intertrial variability (error bars in Figure 4c) are highest for a BOLD correction assuming a mono-exponential T_2*-decay. VASO signal time course with TE = 14 ms and corrected for BOLD with dynamic division shows smallest intertrial variability.

In GM voxels containing more than 10% partial volume of CSF, the BOLD signal change is larger compared with GM voxels that do not have partial volume of CSF ($P < 0.001$) (Fig. 8). On the other hand, VASO signal change is significantly ($P < 0.05$) smaller in such voxels.

The effect of inflow of fresh blood on VASO is examined in three subjects with different TI1 = 760/1120/1330 ms during hypercapnia induced by breathing a gas mixture containing 5% CO_2 (Fig. 9). These results demonstrate the effect of inflow of fresh blood during the blood-nulling time and how these inflow effects can be minimized. With a long blood-nulling time of 1330 ms, the majority of GM voxels show VASO signal increase, suggesting inflow of fresh, noninverted, blood magnetization (blue voxels in Figure 9). The number of these voxels is minimized by decreasing TI1, when the arterial arrival time is shorter than the blood-nulling time.

Table 1
Results of All 10 Subjects that Were Scanned at 7T[a]

Subject	Sex	$\frac{\Delta CBV}{CBV_{rest}}$	Activated volume in cm^3	GM fraction
1	m	30.6%	8.5	61%
2	m	27.9%	4.8	61%
3	w	28.5%	9.5	61%
4	m	20.8%	5.9	51%
5	m	23.6%	6.0	64%
6	m	33.3%	7.0	57%
7	w	31.7%	9.7	55%
8	w	22.8%	7.7	65%
9	w	33.9%	10.1	55%
10	w	29.2%	9.1	49%
All		28.2% ± 4.5%	7.8 ± 1.8	58% ± 5%
Women		29.2% ± 3.7%	9.2 ± 0.8	57% ± 6%
Men		27.2% ± 4.5%	6.5 ± 1.2	59% ± 5%

[a]Relative CBV changes refer to all voxels within the activation maps.

DISCUSSION

CBV Changes

The measured average change in CBV of 28% ± 5% for visual stimulation is in good agreement with values reported in the literature of human studies using different CBV-sensitive modalities, such as paramagnetic contrast agents, a multi-exponential T_2 model, or positron-emission tomography (39–41) (32% ± 10%, 21% ± 5% and 30% ± 7%).

Intersubject Stability

Despite the fact that VASO CNR is approximately only 60% of BOLD CNR, intersubject variability appears to be smaller in VASO time courses as compared to BOLD time courses, which results in smaller intersubject variability in average VASO signal as shown in Figure 6. The measured coefficients of variation (mean standard deviation of signal at one time point during activity divided by the signal change) are 26.9% and 33.3% for VASO and BOLD, respectively. The greater intersubject stability might be explained by considering that BOLD contrast depends on multiple physiological variables, while VASO depends on CBV change alone. For example, variations in venous baseline oxygenation level affect BOLD signal stability, but do not affect vasculature (42–44). It must be pointed out that the echo time of 19 ms used here is close to the tissue T_2*, which provides optimal sensitivity to BOLD signal change at 7T. The mean T_2* from the GM in the occipital lobe measured in our multi-echo data is 22 ms ± 5 ms. Therefore, it seems unlikely that inferior intersubject stability in the BOLD results is due to suboptimal choice of the acquisition parameters.

Activation Time Courses

Both VASO and BOLD signals return to baseline after a similar time (Fig. 6), contrasting with Mandeville et al. (45), but in agreement with Dechent et al (46), Poser and Norris (47), and the results reviewed in van Zijl et al (48). VASO signal change reflects ΔCBV mostly of arteriolar, capillary blood compartments as long as they are nulled, independent of their oxygenation level. The BOLD effect, on the other hand, is dominated by the most deoxygenated part of the vasculature. Therefore, the fast return to baseline of VASO data does not necessarily contradict predictions made by the balloon or windkessel model (45,49), with the corresponding explanation of BOLD poststimulus undershoot. The fast time scale of CBV change might result from the smallness or indeed absence of changes in venous CBV with short stimulus durations (25).

Dynamic Changes of CSF Volume

Assuming the skull as a container of a fixed volume, increase of one compartment, e.g., CBV, must be compensated by volume decrease in another compartment, e.g., GM or CSF (50). VASO signal change is based on the idea that CBV increase is compensated by GM volume decrease only. However, dependent on the brain region stimulated, a small dynamic change in CSF volume in the range of 0.5% to 10% has been experimentally observed (40,51,52). Such stimulus-dependent variations in CSF volume could cause an incorrect calculation of ΔCBV from the VASO signal change (40,51,53,54).

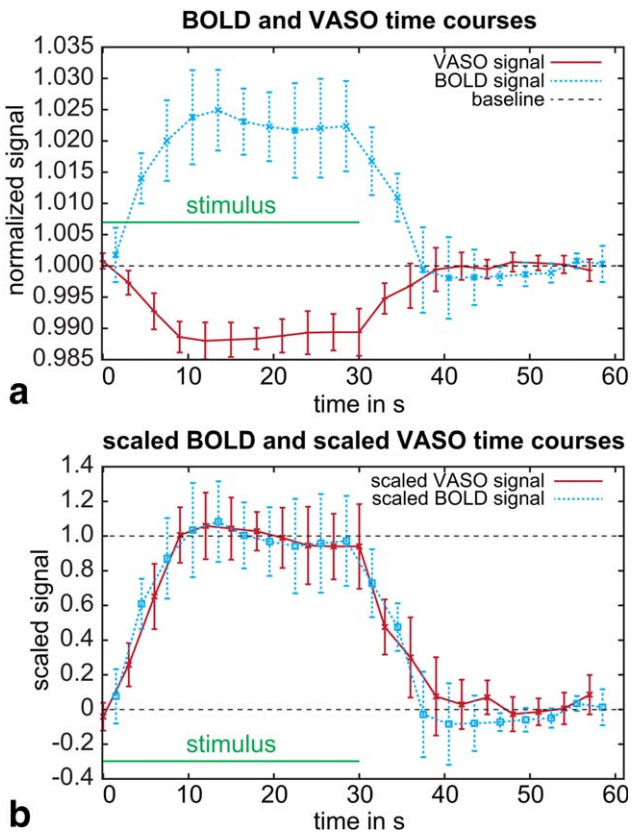

FIG. 6. BOLD and VASO signal time courses. **a:** Normalized signal changes. **b:** Scaled BOLD and VASO signal time courses. Note the similar time scale of the recurrence to baseline in VASO and in BOLD. Note also the smaller intersubject variability in VASO compared with BOLD. [Color figure can be viewed in the online issue, which is available at wileyonlinelibrary.com.]

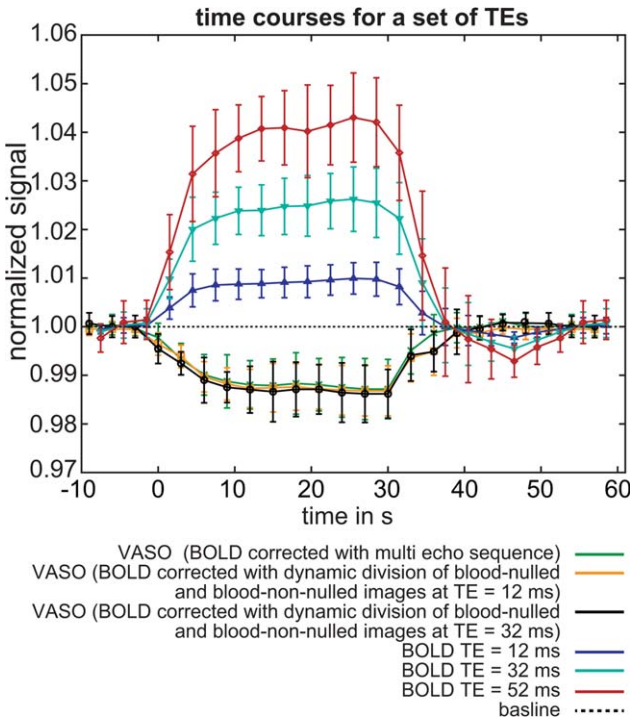

FIG. 7. VASO and BOLD signal responses for different TEs. VASO signal time courses are depicted for different BOLD correction methods. The green line corresponds to BOLD correction with a multi-echo readout. The black/yellow lines correspond to the BOLD correction mechanism that is based on dynamic division of blood-nulled and blood-not-nulled images at TE = 12/32 ms. Error bars refer to standard deviation across subjects. Signal time courses refer to the same stimulation paradigms, but different TEs. [Color figure can be viewed in the online issue, which is available at wileyonlinelibrary.com.]

In SS-SI-VASO, manipulations of the stationary CSF *z*-magnetization can be used to minimize sensitivity to such dynamic changes in CSF volume. In SS-SI-VASO, blood *z*-magnetization is not considered to be in steady-state; hence, the blood-nulling time is independent of TR. Therefore, TR can be adjusted as a free parameter to manipulate the relative signal weighting of GM and CSF. For TR in the order of 3–4 s, the MRI signal intensities of GM and CSF are similar, and the VASO signal change corresponds to changes in both of these compartments, that is, a CBV increase compensated by a GM volume decrease as well as a CBV increase that is compensated with a decrease in CSF volume. If TR is approximately 7 s, both compartments, once-inverted blood and steady-state CSF magnetization, are nulled simultaneously. In this case, VASO signal change reflects only the CBV increase that is compensated by GM decrease, and it is insensitive to CBV increase that is compensated by CSF decrease. Thus, the sensitivity of VASO to dynamic changes in CSF can be modulated in SS-SI-VASO simply by adapting TR, whereas in the original VASO (4), implementations based on more time-inefficient methods like VASO FLAIR (53) or ACDC VASO (51) need to be applied.

Signal Change at the Cortical Surface

The observation that VASO is smaller in GM voxels with significant partial-volume contributions from CSF (see Fig. 8) is consistent with results showing that ΔCBV is smaller in voxels closer to the pial surface, in contrast to BOLD (1,5,55). It suggests that changes in CBV are independent of pial veins, which are known often to dominate the BOLD effect. In fact, such comparisons between CBV (MION and SI-VASO) and BOLD (gradient echo and spin echo) were performed by Jin, Kim, and coworkers (5,55–57) in cats at 9.4T with ultra-high resolution, and the results in Figure 8 can be understood as a low-resolution replication of part of their findings. Note that surface voxels can have different partial-volume characteristics from more typical voxels. This means, independent of the underlying layer-dependency of VASO and BOLD, surface voxels are expected to show smaller signal changes corresponding to the smaller GM volume they contain. However, because BOLD signal changes are investigated in the same subset of voxels, partial-volume biases are identical in BOLD and VASO signal change. Therefore, differences between BOLD and VASO can be considered independent of such biases.

BOLD Correction Mechanism

The proposed BOLD correction scheme based on a dynamic division of images with and without blood nulling is compared with an alternative previously established BOLD correction based on a mono-exponential T_2* decay in a multi-echo EPI readout (see Figure 7 for 7T data). The concordance in amplitude and temporal characteristics suggests that BOLD correction with dynamic division can account for BOLD contamination as accurately as BOLD correction with multi-echo acquisition. It is further validated by a comparison of results obtained at 3T with different echo times of 14 and 30 ms, where BOLD contaminations are expected to be smaller (8) (Fig. 4c).

Inflow of Noninverted Blood Magnetization During TI1 into Arterial Vessels

Inflow of noninverted blood can introduce a CBF-weighting that counteracts the SS-SI-VASO contrast (see Figure 9 with long TI1). However, if TI1 is made smaller than the arterial arrival time, this effect can be avoided (see Figure 9 at short TI1).

Blood Magnetization in Venous Vessels

Due to the finite permeability of capillary walls, downstream vascular compartments can be filled with a mixture of arterial water and tissue water. Hence venous blood magnetization might not be completely nulled and its contribution to the functional VASO contrast is underestimated (4,5). In case the refilling condition of SS-SI-VASO is violated and steady-state blood in the microvasculature has not been completely replaced by fresh once-inverted blood, the blood magnetization of the corresponding downstream vessels would not be completely nulled. Due to both of these effects, the contribution of venous CBV change can be underestimated even though the venous CBV change is expected to be small (5,58,59).

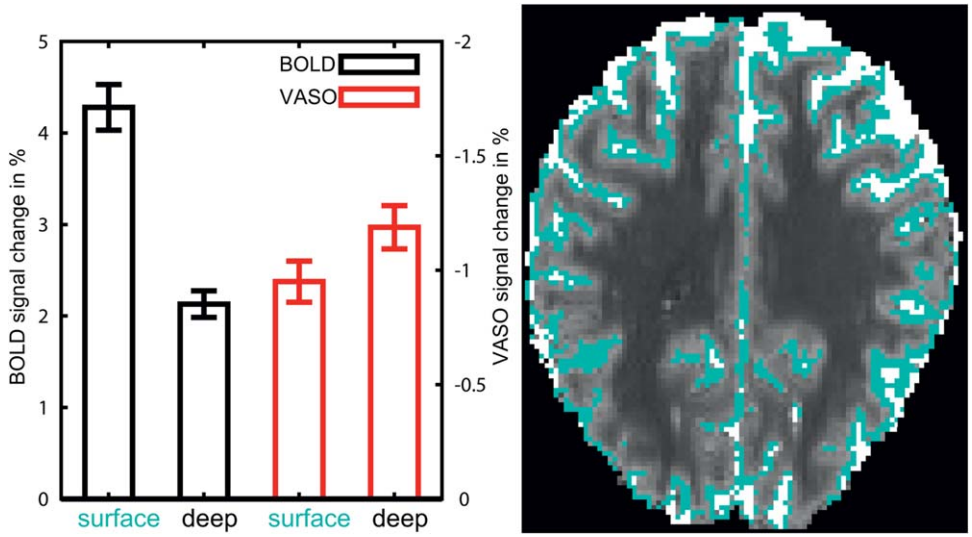

FIG. 8. VASO and BOLD signal changes in gray matter surface voxels compared with signal change in voxels representing deeper cortical layers of the visual cortex. The BOLD signal change is dominated from surface voxels and VASO signal change is smaller in surface voxels compared with deeper voxels. Error bars refer to the standard error of mean across 10 subjects. This discrepancy might reflect the different vascular origin of BOLD and VASO. A representative map of such surface voxels across a slice through the brain is depicted on the right. [Color figure can be viewed in the online issue, which is available at wileyonlinelibrary.com.]

Magnetization Exchange Between Intra- and Extravascular Spaces

Similar to the original VASO, SS-SI-VASO is based on a model of two nonexchanging compartments. However, magnetization exchange between intra- and extravascular spaces due to finite permeability of the capillary wall can result in CBF-dependent reduction of the GM signal (4,60). In SS-SI-VASO, the magnetization within the slice is kept at a low value during inversion. Hence, during the entire period III inverted blood magnetization will enter the slice and exchange with tissue magnetization that is close to zero. The large difference between blood and tissue magnetization is a unique feature of SS-SI-VASO. Due to this difference, the *absolute* exchange of magnetic moment (i.e., in units of A m^2) between intravascular and extravascular space will be larger than in original VASO. The increase in sensitivity of SS-SI-VASO compared with original VASO, hence, appears to come at the price of increased sensitivity to perfusion. However, the tissue signal in SS-SI-VASO still exceeds that of original VASO by approximately an order of magnitude. So, we consider it likely that the *relative* perfusion contribution (in percent of the SS-SI-VASO signal) will be comparable to the relative perfusion contribution in original VASO (60). Detailed studies, including multicompartment simulations, will be required to estimate the magnitudes of absolute and relative perfusion contributions in SS-SI-VASO.

Extensibility to a Three-Dimensional Method

VASO has been extended to a multi-slice method with several advanced readout strategies (6,47,54,61–63), or

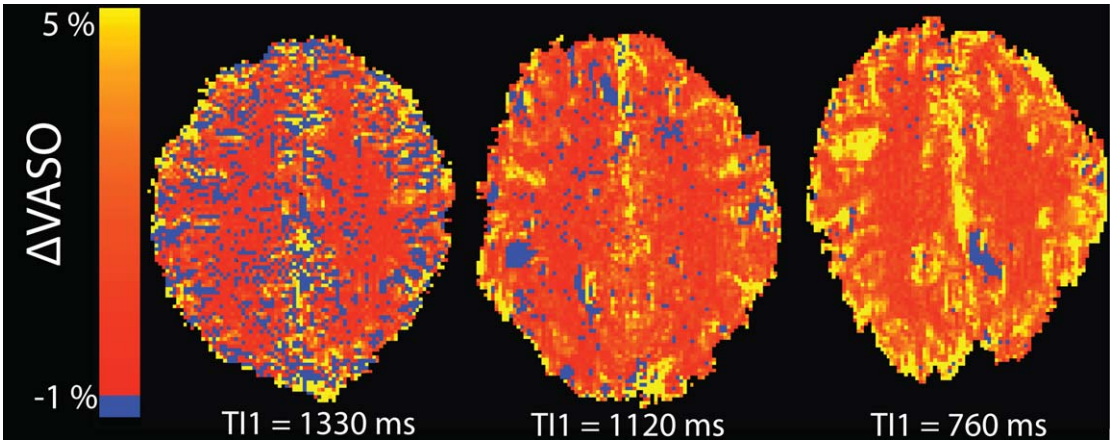

FIG. 9. Maps of VASO signal change in three different subjects with TI1 = 760/1120/1330 ms during hypercapnia. Voxels with significant VASO signal increase due to inflow of fresh blood magnetization during hypercapnia are depicted in blue. The number of these voxels decreases with shorter blood-nulling times, as inflow effects of fresh blood are reduced. [Color figure can be viewed in the online issue, which is available at wileyonlinelibrary.com.]

by means of advanced modeling (64). In SS-SI-VASO, these methods can be used to increase the number of imaging slices, analogously. The additional requirements of the SS-SI-VASO regarding the vasculature dynamics must be considered in adjusting the sequence parameters when it is applied with a three-dimensional acquisition. For example, if more imaging slices have to be acquired, TR must increase to give blood sufficient time to refill the vasculature between consecutive image acquisitions, and of course both the imaging slab thickness and the inversion slab thickness must be increased. Alternatively, the blood nulling time could be reduced, by means of smaller inversion efficiency, to prevent inflow effects of fresh blood into the imaging slab. The fundamental limitations of the imaging slab thickness in slab-selective VASO are comparable to limitations of pulsed arterial spin labeling (PASL) methods (65), which are also given by refilling behavior of the vasculature within a slab.

CONCLUSIONS

We have shown that the proposed SS-SI-VASO yields reliable and consistent detection of CBV changes in humans at 7T. Here, blood arrival and transit times of healthy subjects are comparable to the blood-nulling time after inversion, which is used in a slab-selective approach to increase the functional CNR. With these improvements, SS-SI-VASO may be a useful tool for high-resolution functional brain mapping in humans at high fields. Furthermore, the high sensitivity of the proposed method can play an important role in neuroscientific research, where experiments are limited by low SNR, e.g., investigating neurovascular coupling in negative BOLD regions (66,67), or in calibrated BOLD fMRI (68).

ACKNOWLEDGMENTS

We thank Domenica Wilfling and Elisabeth Wladimirow for experimental assistance. We thank Dr. Ilona Henseler, Dr. Elisabeth Roggenhofer, and Dr. Stephan Kabisch for medical supervision of experiments with hypercapnia. We thank Dr. Alexis Amadon for sharing his MAFI sequence code that was used for $B1^+$-mapping. We thank Dr. Olaf Dietrich and Dr. Walter Assmann for helpful discussions. Preliminary accounts of this work have been presented in the Proceedings of the 20th Annual Meeting of ISMRM, Melbourne, Australia, 2012. (abstract 381).

REFERENCES

1. Kim T, Kim SG. Temporal dynamics and spatial specificity of arterial and venous blood volume changes during visual stimulation: implication for BOLD quantification. J Cereb Blood Flow Metab 2010;12:1211–1222.
2. Lu H, Patel S, Luo F, Li SJ, Hillard CJ, Ward BD, Hyde JS. Spatial correlations of laminar BOLD and CBV responses to rat whisker stimulation with neuronal activity localized by Fos expression. Magn Reson Med 2004;52:1060–1068.
3. Kennerley AJ, Mayhew JE, Redgrave P, Berwick J. Vascular origins of BOLD and CBV fMRI signals: statistical mapping and histological sections compared. Open Neuroimag J 2010;4:1–8.
4. Lu H, Golay X, Pekar JJ, van Zijl PCM. Functional magnetic resonance imaging based on changes in vascular space occupancy. Magn Reson Med 2003;50:263–274.
5. Jin T, Kim S-G. Improved cortical-layer specificity of vascular space occupancy fMRI with slab inversion relative to spin-echo BOLD at 9.4T. Neuroimage 2008;40:59–67.
6. Hua J, Jones CK, Qin Q, van Zijl PC. Implementation of vascular-space-occupancy MRI at 7T. Magn Reson Med 2013;69:1003–1013.
7. Rooney WD, Johnson G, Li X, Cohen ER, Kim S-G, Ugurbil K, Springer CS. Magnetic field and tissue dependencies of human brain longitudinal H2O relaxation in vivo. Magn Reson Med 2007;57:308–318.
8. Lu H, van Zijl PCM. Experimental measurement of extravascular parenchymal BOLD effect and tissue oxygen extraction fraction using multi-echo VASO fMRI at 1.5 and 3.0 T. Magn Reson Med 2005;53:808–816.
9. Hetzer S, Mildner T, Moller HE. A modified EPI sequence for high-resolution imaging at ultra-short echo time. Magn Reson Med 2011;65:165–175.
10. Hua J, Donahue MJ, Zhao JM, Grgac K, Huang AJ, Zhou J, van Zijl PC. Magnetization transfer enhanced vascular-space-occupancy (MT-VASO) functional MRI. Magn Reson Med 2009;61:944–951.
11. Wu WC, Buxton RB, Wong EC. Vascular space occupancy weighted imaging with control of residual blood signal and higher contrast-to-noise ratio. IEEE Trans Med Imaging 2007;26:1319–1327.
12. Wu CW, Chuang KH, Wai YY, Wan YL, Chen JH, Liu HL. Vascular space occupancy-dependent functional MRI by tissue suppression. J Magn Reson Imaging 2008;28:219–226.
13. Shen Y, Kauppinen RA, Vidyasagar R, Golay X. A functional magnetic resonance imaging technique based on nulling extravascular gray matter signal. J Cereb Blood Flow Metab 2009;29:144–156.
14. Jin T, Kim SG. Spatial dependence of CBV-fMRI: a comparison between VASO and contrast agent based methods. Conf Proc IEEE Eng Med Biol Soc 2006;1:25–28.
15. Kim SG. Quantification of relative cerebral blood-Flow change by flow-sensitive alternating inversion-recovery (FAIR) technique - application to functional mapping. Magn Reson Med 1995;34:293–301.
16. Dobre MC, Ugurbil K, Marjanska M. Determination of longitudinal relaxation time (T1) at high magnetic field strengths. Magn Reson Imaging 2006;25:733–735.
17. Grgac K, van Zijl PC, Qin Q. Hematocrit and oxygenation dependence of blood (1) H(2) O T(1) at 7 tesla. Magn Reson Med 2013;70:1153–1159.
18. Zhang X, Petersen ET, Ghariq E, De Vis JB, Webb AG, Teeuwisse WM, Hendrikse J, van Osch MJ. In vivo blood T(1) measurements at 1.5 T, 3 T, and 7 T. Magn Reson Med 2013;70:1082–1086.
19. Francis ST, Bowtell RW, Gowland PA. Modeling and optimization of look-locker spin labeling for measuring perfusion and transit time changes in activation studies taking into account arterial blood volume. Magn Reson Imaging 2008;59:316–325.
20. Wong EC, Buxton R, Frank LR. Implementation of quantitative perfusion imaging techniques for functional brain mapping using pulsed arterial spin labeling. NMR Biomed 1997;10:237–249.
21. Chen Y, Wang DJ, Detre JA. Comparison of arterial transit times estimated using arterial spin labeling. MAGMA 2012;25:135–144.
22. Norris DG, Haase A. Variable excitation angle AFP pulses. Magn Reson Med 1989;9:435–440.
23. Pawlik G, Rackl A, Bing RJ. Quantitative capillary topography and blood flow in the cerebral cortex of cats: an in vivo microscopic study. Brain Res 1981;208:35–58.
24. Kleinfeld D, Mitra PP, Helmchen F, Denk W. Fluctuations and stimulus-induced changes in blood flow observed in individual capillaries in layers 2 through 4 of rat neocortex. Proc Natl Acad Sci U S A 1998;95:15741.
25. Hillman EMC, Devor A, Bouchard MB, Dunn AK, Krauss GW, Skoch J, Bacskai BJ, Dale AM, Boas DA. Depth-resolved optical imaging and microscopy of vascular compartment dynamics during somatosensory stimulation. Neuroimage 2007;35:89–104.
26. Nakagawa H, Lin S-Z, Bereczki D, Gesztelyi G, Otsuka T, Wei L, Hans F-J, Acuff VR, Chen J-L, Pettigrew KD, et al. Blood volumes, hematocrits, and transit-times in parenchymal microvascular systems of the rat brain. In: Denis LB, editor. Diffusion and perfusion magnetic resonance imaging: application to functional MRI. New York: Raven Press; 1995. p 193–204.

27. Jespersen SN, Ostergaard L. The roles of cerebral blood flow, capillary transit time heterogeneity, and oxygen tension in brain oxygenation and metabolism. J Cereb Blood Flow Metab 2012;32:264–277.
28. Lu H, Hua J, van Zijl PC. Noninvasive functional imaging of cerebral blood volume with vascular-space-occupancy (VASO) MRI. NMR Biomed 2013;26:932–948.
29. Donahue MJ, Hoogduin H, van Zijl PC, Jezzard P, Luijten PR, Hendrikse J. Blood oxygenation level-dependent (BOLD) total and extravascular signal changes and DeltaR2* in human visual cortex at 1.5, 3.0 and 7.0 T. NMR Biomed 2011;24:25–34.
30. Martindale J, Kennerley AJ, Johnston D, Zheng Y, Mayhew JE. Theory and generalization of Monte Carlo models of the BOLD signal source. Magn Reson Med 2008;59:607–618.
31. Hurley AC, Al-Radaideh A, Bai L, Aickelin U, Coxon R, Glover P, Gowland PA. Tailored RF pulse for magnetization inversion at ultrahigh field. Magn Reson Med 2010;63:51–58.
32. Shin W, Geng X, Gu H, Zhan W, Zou Q, Yang Y. Automated brain tissue segmentation based on fractional signal mapping from inversion recovery Look-Locker acquisition. Neuroimage 2010;52: 1347–1354.
33. Huk AC, Dougherty RF, Heeger DJ. Retinotopy and functional subdivision of human areas MT and MST. J Neurosci 2002;22: 7195–7205.
34. Ho Y-CL, Peterson RT, Zimine I, Golay X. Similarities and differences in arterial responses to hypercapnia and visual stimulation. J Cereb Blood Flow Metab 2011;31:560–571.
35. Worsley KJ. Statistical analysis of activation images. In: Jezzard P, Matthews PM, Smith SM, editors. Functional Magnetic Resonance Imaging: An Introduction to Methods. UK: Oxford University Press; 2001.
36. Jochimsen TH, von Mengershausen M. ODIN-object-oriented development interface for NMR. J Magn Reson 2004;170:67–78.
37. Lu H, Law M, Johnson G, Ge Y, van Zijl PCM. Novel approach to the measurement of absolute cerebral blood volume using vascular-space-occupancy magnetic resonance imaging. Magn Reson Med 2005;54: 1403–1411.
38. Giovacchini G, Chang MC, Channing MA, et al. Brain incorporation of 11c-arachidonic acid in young healthy humans measured with positron emission tomography. J Cereb Blood Flow Metab 2002;22: 1453–1462.
39. Belliveau JW, Kennedy DN, McKinstry RC, Buchbinder BR, Weisskoff RM, Cohen MS, Vevea JM, Brady TJ, Rosen BR. Functional mapping of the human visual cortex by magnetic resonance imaging. Science 1991;254:716–719.
40. Piechnik SK, Evans J, Bary LH, Wise RG, Jezzard P. Functional changes in CSF volume estimated using measurement of water T2 relaxation. Magn Reson Imaging 2009;61:579–586.
41. Ito H, Takahashi K, Hatazawa J, Kim S-G, Kanno I. Changes in human regional cerebral blood flow and cerebral blood volume during visual stimulation measured by positron emission tomography. J Cereb Blood Flow Metab 2001;21:608–612.
42. Lu H, Zhao C, Ge Y, Lewis-Amezcua K. Baseline blood oxygenation modulates response amplitude: physiologic basis for intersubject variations in functional MRI signals. Magn Reson Med 2008;60: 364–372.
43. Tjandra T, Brooks JCW, Figueiredo P, Wise R, Matthews PM, Tracey I. Quantitative assessment of the reproducibility of functional activation measured with BOLD and MR perfusion imaging: implications for clinical trial design. Neuroimage 2005;27:393–401.
44. Leontiev O, Buxton RB. Reproducibility of BOLD, perfusion, and CMRO2 measurements with calibrated-BOLD fMRI. Neuroimage 2007;35:175–184.
45. Mandeville JB, Marota JJ, Ayata C, Zaharchuk G, Moskowitz MA, Rosen BR, Weisskoff RM. Evidence of a cerebrovascular postarteriole windkessel with delayed compliance. J Cereb Blood Flow Metab 1999;19:679–689.
46. Dechent P, Schuetze G, Helms G, Merboldt KD, Frahm J. Basal cerebral blood volume during the poststimulation undershoot in BOLD MRI of the human brain. J Cereb Blood Flow Metab 2010;31: 82–89.
47. Poser BA, Norris DG. Measurement of activation-related changes in cerebral blood volume: VASO with single-shot HASTE acquisition. Magn Reson Mater Phys 2007;20:63–67.
48. van Zijl PC, Hua J, Lu H. The BOLD post-stimulus undershoot, one of the most debated issues in fMRI. Neuroimage 2012;62:1092–1102.
49. Buxton RB, Wong EC, Frank LR. Dynamics of blood flow and oxygenation changes during brain activation: the balloon model. Magn Reson Med 1998;39:855–864.
50. Morki B. The Monro-Kellie hypothesis: applications in CSF volume depletion. Neurology 2001;56:1746–1748.
51. Scouten A, Constable RT. VASO-based calculations of CBV change: accounting for the dynamic CSF volume. Magn Reson Med 2008;58: 308–315.
52. Jin T, Kim SG. Change of the cerebrospinal fluid volume during brain activation investigated by T(1rho)-weighted fMRI. Neuroimage 2010; 51:1378–1383.
53. Donahue MJ, Lu H, Jones CK, Edden RA, Pekar JJ, van Zijl PC. Theoretical and experimental investigation of the VASO contrast mechanism. Magn Reson Med 2006;56:1261–1273.
54. Scouten A, Constable RT. Application and limitations of whole-brain MAGIC VASO fuctional fmaging. Magn Reson Med 2007;58:306–315.
55. Jin T, Kim SG. Cortical layer-dependent dynamic blood oxygenation, cerebral blood flow and cerebral blood volume responses during visual stimulation. Neuroimage 2008;43:1–9.
56. Zhao F, Jin T, Wang P, Hu X, Kim SG. Sources of phase changes in BOLD and CBV-weighted fMRI. Magn Reson Med 2007;57:520–527.
57. Kim SG, Harel N, Jin T, Kim T, Lee P, Zhao F. Cerebral blood volume MRI with intravascular superparamagnetic iron oxide nanoparticles. NMR Biomed 2013;26:949–962.
58. Kennerley AJ, Berwick J, Martindale J, Johnston D, Papadakis N, Mayhew JE. Concurrent fMRI and optical measures for the investigation of the hemodynamic response function. Magn Reson Med 2005; 54:354–365.
59. Kim T, Hendrich KS, Masamoto K, Kim SG. Arterial versus total blood volume changes during neural activity-induced cerebral blood flow change: implication for BOLD fMRI. J Cereb Blood Flow Metab 2007;27:1235–1247.
60. Wu CW, Liu H-L, Chen J-H, Yang Y. Effects of CBV, CSF, and blood-brain barrier permeability on accuracy of PASL and VASO measurement. Magn Reson Med 2010;63:601–608.
61. Poser BA, Norris DG. 3D single-shot VASO using a Maxwell gradient compensated GRASE sequence. Magn Reson Med 2009;62:255–262.
62. Donahue MJ, Blicher JU, Ostergaard L, Feinberg DA, MacIntosh BJ, Miller KL, Gunther M, Jezzard P. Cerebral blood flow, blood volume, and oxygen metabolism dynamics in human visual and motor cortex as measured by whole-brain multi-modal magnetic resonance imaging. J Cereb Blood Flow Metab 2009;29:1856–1866.
63. Poser BA, Norris DG. Application of whole-brain CBV-weighted fMRI to a cognitive stimulation paradigm: robust activation detection in a stroop task experiment using 3D GRASE VASO. Hum Brain Mapp 2011;32:974–981.
64. Ciris PA, Qiu M, Constable TR. Non-invasive quantification of absolute cerebral blood volume applicable to the whole human brain. In Proceedings of the 20th Annual Meeting of ISMRM, Melbourne, Australia, 2012. Abstract 381.
65. Calamante F, Thomas DL, Pell GS, Wiersma J, Turner R. Measuring cerebral blood flow using magnetic resonance imaging techniques. J Cereb Blood Flow Metab 1999;19:701–735.
66. Huber L, Goense J, Ivanov D, Krieger SN, Turner R, Möller HE. Cerebral blood volume changes in negative BOLD regions during visual stimulation in humans at 7T. In Proceedings of the 21st Annual Meeting of ISMRM, Salt Lake Citiy, Utah, 2013. Abstract 918.
67. Goense J, Merkle H, Logothetis NK. High-resolution fMRI reveals laminar differences in neurovascular coupling between positive and negative BOLD responses. Neuron 2012;76:629–639.
68. Huber L, Ivanov D, Krieger SN, Gauthier C, Roggenhofer E, Henseler I, Turner R, Moller HE. Measurements of cerebral blood volume and BOLD signal during hypercapnia and functional stimulation in humans at 7T: application to calibrated BOLD. In Proceedings of the 21st Annual Meeting of ISMRM, Salt Lake Citiy, Utah, USA, 2013. Abstract 918.